Bioactive Materials 30 (2023) 29–45

Contents lists available at ScienceDirect

Bioactive Materials

journal homepage: www.keaipublishing.com/en/journals/bioactive-materials

Glucose-responsive, antioxidative HA-PBA-FA/EN106 hydrogel enhanced diabetic wound healing through modulation of FEM1b-FNIP1 axis and promoting angiogenesis

Wenqian Zhang [a,b,1], Kangkang Zha [a,b,1], Yuan Xiong [a,b,1], Weixian Hu [a,b,1], Lang Chen [a,b], Ze Lin [a,b], Chenyan Yu [a,b], Wu Zhou [a,b], Faqi Cao [a,b], Hankun Hu [c,d,e,***], Bobin Mi [a,b,**], Guohui Liu [a,b,*]

[a] Department of Orthopaedics, Union Hospital, Tongji Medical College, Huazhong University of Science and Technology, Wuhan, 430022, China
[b] Hubei Province Key Laboratory of Oral and Maxillofacial Development and Regeneration, Wuhan, 430022, China
[c] Department of Pharmacy, Zhongnan Hospital of Wuhan University, School of Pharmaceutical Sciences, Wuhan University, Wuhan 430071, China
[d] Hubei Micro-explore Innovative Pharmaceutical Research Co, Ltd, Wuhan, Hubei, 430071, PR China
[e] Suzhou Organ-on-a-Chip System Science and Technology Co, Ltd, Suzhou, Jiangsu, 215000, PR China

ARTICLE INFO

Keywords:
FNIP1
Wound healing
Hydrogel
Antioxidant
Glucose-responsive

ABSTRACT

The diabetic wounds remain to be unsettled clinically, with chronic wounds characterized by drug-resistant bacterial infections, compromised angiogenesis and oxidative damage to the microenvironment. To ameliorate oxidative stress and applying antioxidant treatment in the wound site, we explore the function of folliculin-interacting protein 1 (FNIP1), a mitochondrial gatekeeper protein works to alter mitochondrial morphology, reduce oxidative phosphorylation and protect cells from unwarranted ROS accumulation. And our *in vitro* experiments showed the effects of FNIP1 in ameliorating oxidative stress and rescued impaired angiogenesis of HUVECs in high glucose environment. To realize the drug delivery and local regulation of FNIP1 in diabetic wound sites, a novel designed glucose-responsive HA-PBA-FA/EN106 hydrogel is introduced for improving diabetic wound healing. Due to the dynamic phenylboronate ester structure with a phenylboronic acid group between hyaluronic acid (HA) and phenylboronic acid (PBA), the hydrogel is able to realize a glucose-responsive release of drugs. Fulvic acid (FA) is added in the hydrogel, which not only severs as crosslinking agent but also provides antibacterial and anti-inflammatory abilities. Moreover, the release of FEM1b-FNIP1 axis inhibitor EN106 ameliorated oxidative stress and stimulated angiogenesis through FEM1b-FNIP1 axis regulation. These *in vivo* and *in vitro* results demonstrated that accelerated diabetic wounds repair with the use of the HA-PBA-FA/EN106 hydrogel, which may provide a promising strategy for chronic diabetic wound repair.

1. Introduction

Diabetes is one of the fastest growing diseases worldwide, which leads to devastating macrovascular and microvascular complications [1]. Chronic non-healing wounds are a major complication of diabetes, which affects 1 in 10 people worldwide [2]. Diabetic wounds, characterized by drug-resistant bacterial infections, biofilm formation, compromised angiogenesis and wound perfusion, perpetuating inflammation, and oxidative damage to the microenvironment, need to settle many environmental and intrinsic factors associated with diabetes mellitus [3]. These factors pose great challenges to the dressing design for diabetic wounds.

Peer review under responsibility of KeAi Communications Co., Ltd.

* Corresponding author. Department of Orthopedics, Union Hospital, Tongji Medical College, Huazhong University of Science and Technology, 1277 Jiefang Avenue, Wuhan, 430022, China.

** Corresponding author. Department of Orthopedics, Union Hospital, Tongji Medical College, Huazhong University of Science and Technology, 1277 Jiefang Avenue, Wuhan, 430022, China.

*** Corresponding author. Department of Pharmacy, Zhongnan Hospital of Wuhan University, Wuhan, Hubei, 430071, China.

E-mail addresses: huhankun@whu.edu.cn (H. Hu), mibobin@hust.edu.cn (B. Mi), liuguohui@hust.edu.cn (G. Liu).

[1] These authors contributed equally to this article.

https://doi.org/10.1016/j.bioactmat.2023.07.006
Received 14 April 2023; Received in revised form 2 July 2023; Accepted 5 July 2023

Hydrogels, consisting of natural or synthetic hydrophilic polymer chains connected to each other at the crosslinking point, demonstrate their promise in wound healing for their excel qualities in biophysical and biochemical properties such as the matrix mechanics, degradability, microstructure, cell adhesion, and cell-cell interactions [4]. Given the variability and complexity of the physiological environment in the body, it remains to be a challenge of designing a delivery system that is sensitive to the change of metabolic state in the body, especially to the hyperglycemia in diabetic wounds [5].

To address the high glucose environment of diabetic wound sites, hydrogels applying the dynamic phenylboronate ester structure with a phenylboronic acid group draws universal attention, which possess catechol structure and has been widely proved to behave in a glucose-responsive degradation manner [6,7].

Excessive inflammatory infiltration impedes the histological repair of the diabetic wound in a predictable biological step and chronological order [8]. Therefore, resolving excessive inflammation in diabetic wound healing is crucial [9]. Besides, high blood glucose levels in diabetic wound sites can lead to faster growth of bacteria than normal wounds [10], and multidrug-resistant bacterial infection further limit the use of many hydrogel-based therapies in diabetic wound healing [11,12]. Natural health products (NHPs) have been considered as a promising way to address these challenges such as fulvic acid (FA), which comes from humic substances produced by microorganisms in soil. Traditional medicine and modern research claim FA can modulate the immune system, influence the oxidative state of cells, and improve gastrointestinal function; all of which are hallmarks of diabetes [13]. Besides, FA has been reported as a promising topical remedy for drug-resistant wound infections, which accelerated the healing process of wounds infected with methicillin-resistant *S. aureus* and multidrug-resistant *P. aeruginosa* in rats [14,15]. Therefore, FA possesses both antimicrobial and anti-inflammatory properties, which are crucial for wound healing dress.

Oxidative stress is another crucial issue impairing the restoration of diabetic wounds that need to be handled [16]. Oxidative stress refers to an imbalance between production of oxidants and antioxidant defenses that may result in damage to biological systems, which has been proved as one of the disadvantage factors in the diabetic wound healing process [17]. Oxidative stress contributes to the damage of diabetic wound healing could be attributed to two major mechanisms. The first mechanism involves the production of reactive oxygen species (ROS), which directly oxidize macromolecules, including membrane lipids, structural proteins, enzymes and nucleic acids, leading to impaired cell function and cell death [18]. The second mechanism of oxidative stress is aberrant redox signaling. In oxidative stress, non-physiological production of ROS, such as H2O2, can result in abnormal redox signaling [19]. In recent years, FEM1b-FNIP1 axis has been newly founded to participate in redox signaling [20]. Folliculin-interacting protein 1 (FNIP1), which has been newly proved as a mitochondrial gatekeeper protein, works to alter mitochondrial morphology, reduce oxidative phosphorylation and protect cells from unwarranted ROS accumulation [21]. FNIP1 stabilization has been considered to contribute to antioxidant defenses in cells with highly active mitochondria. In cell oxidative stress state, loss of FNIP1 increases mitochondrial activity and triggers production of ROS to counteract reductive stress. In cell reductive stress state, the E3 ligase $CUL2^{FEM1B}$ ubiquitylates reduced FNIP1 to trigger its proteasomal degradation, which allows cells to re-activate oxidative phosphorylation and replenish their ROS supply. Besides, FEM1b-FNIP1 axis also has been proved to crosslink with KEAP1-NRF2 signaling pathway to regulate redox balance inside cells [21]. Therefore, regulatory circuit of FEM1b-FNIP1 has been considered to provide opportunities to exploit mitochondrial regulation as a therapeutic approach to diseases of aberrant tissue homeostasis such as diabetes mellitus [20]. However, whether FEM1b-FNIP1 axis participates in the regulation of oxidative stress in diabetic wound sites and what role the FNIP1 plays in the pathological process of diabetic wound healing have not been researched yet. In this study, we focused on the prove of FNIP1 functions in oxidative stress and angiogenesis as well as regulation of FEM1b-FNIP1 axis to ameliorate oxidative stress in diabetic wound healing.

Finally, to realize the drug delivery and local regulation of FNIP1 in diabetic wound sites, a glucose responsive specific EN106 released multifunctional HA-PBA-FA/EN106 hydrogel dressing was prepared via the dynamic phenylboronate ester structure with a phenylboronic acid group between hyaluronic acid (HA) and phenylboronic acid (PBA). In addition, fulvic acid (FA) was added to serve as a crosslinking agent as well as provide anti-inflammation ability. Besides, we introduced EN106, the FEM1b-targeting cysteine-reactive covalent ligand, to regulate FEM1b-FNIP1 axis. The mechanical properties, *in vitro* EN106 release in response to glucose, antibacterial, antioxidant, and biocompatibility of hydrogels were evaluated. Finally, a mice model of type II diabetes was established, and the effect of HA-FA-EN106 hydrogel on promoting diabetic wound healing was examined. In conclusion, HA-FA-EN106 hydrogels with glucose-responsive EN106 release ability, enhanced adhesion, anti-inflammation and antioxidant ability have been proved to have a promoting effect in the healing of chronic diabetic wounds.

2. Results

2.1. High-glucose environment decreased FNIP1 expression

It has been proved that FNIP1 stabilization contribute to antioxidant defenses in cells (Fig. 1A). To verify whether FNIP1 expresses in cells participated in wound healing process, a gene expression analysis was performed. Result showed that besides immune-related cells, over medium abundance of FNIP1 was expressed in cells participated in wound healing process such as HUVECs and keratinocytes (Fig. 1B). To further verify the function of FNIP1 a protein interaction analysis was performed. Result showed that FNIP1 interacted with significant nodes that participated in redox regulation such as DEPDC5, AKT1S1 (Fig. 1C).

Then, whether high-glucose environment alters the FNIP1 expression of cultured HUVECs and diabetic mice wounds were evaluated. After high-glucose cultivation of HUVECs for 72 h, the FNIP1 expression significantly decreased in a dose-dependent manner as compared with control (Fig. 1D). Similar trend was observed at a protein level in diabetic mice wounds (Fig. 1E). Collectively, these data suggested that FNIP1 gene differential expression might be one of the factors that resulted in delayed diabetic wound healing.

2.2. FNIP1 participated in antioxidant defenses of HUVECs

To verify whether FNIP1 participated in antioxidant defenses of HUVECs, we regulated the expression of FNIP1 followed with applying SOD activity kit, MDA kit and ROS indicator DCFH-DA (2'',7''-Dichlorodihydrofluorescein diacetate) to evaluate oxidative stress inside cells.

Firstly, we used the small interfering RNA FNIP1 (siFNIP1) to downregulate the expression of FNIP1. The MDA content was significantly increased in the small interfering RNA FNIP1 (siFNIP1) group compared with control group and the small interfering RNA negative control (siNC) group (Fig. 2A). The SOD activity was significantly decreased in siFNIP1 group (Fig. 2B). And fluorescence intensity of ROS was significantly increased in siFNIP1 group (Fig. 2C). Besides, results of western blotting showed that inflammation and oxidative stress related NFκB signalling pathway was activated in siFNIP1 group (Fig. 2D). Secondly, we applied plasmid transfection to overexpress FNIP1 to verify whether FNIP1 protects HUVECs from high-glucose-induced oxidative stress. The MDA content was significantly decreased in the FNIP1 plasmid transfection (FNIP1) group compared with high glucose group and the negative control plasmid transfection (NC) group (Fig. 2E). The SOD activity was significantly increased in FNIP1 group (Fig. 2F). And fluorescence intensity of ROS was significantly decreased

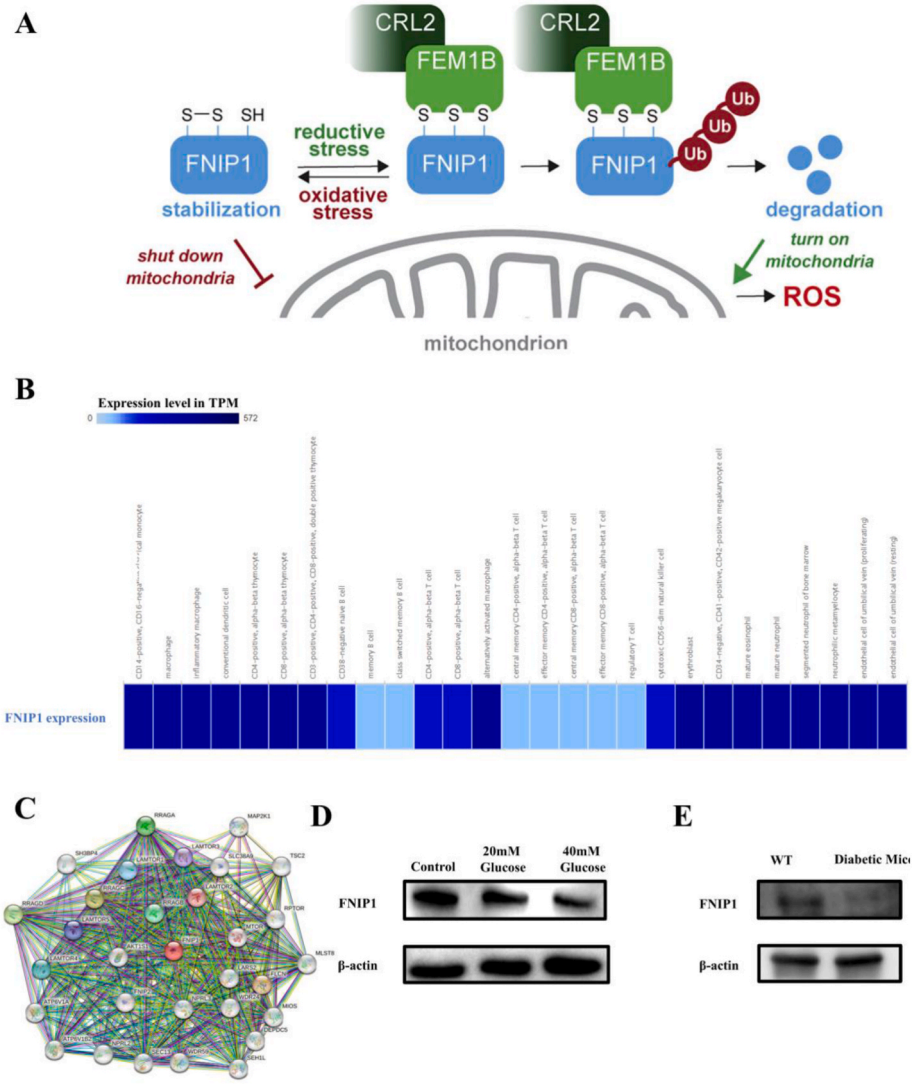

Fig. 1. High-glucose environment decreased FNIP1 expression. (A) Schematic illustration of FNIP1 involved in redox balance regulation. Copyright 2020, Elsevier. (B) Gene expression analysis of FNIP1. (C) Protein interaction networks of FNIP1. (D) Western blotting results of FNIP1 expression in the HUVECs following different treatments. (E) Western blotting results of FNIP1 expression in the skins of wild type mice and diabetic mice.

in FNIP1 group (Fig. 2G). Besides, results of western blotting showed that overexpression of FNIP1 downregulated the activation of NFκB signalling pathway (Fig. 2H).

Together, these findings indicated that FNIP1 participated in anti-oxidant defenses of HUVECs.

2.3. Downregulation of FNIP1 inhibited angiogenesis of HUVECs

To verify whether FNIP1 regulated angiogenesis of HUVECs, we downregulated the expression of FNIP1 and then evaluated proliferation, migration, and tube formation capabilities of treated HUVECs. Firstly, our data also showed that the downregulating of FNIP1 in HUVECs decreased expression of cell cycle-related mRNAs and proteins (Fig. 3A and B), inhibiting cell entry to the S stage (Fig. 3C and D). Then, we performed CCK8 tests to evaluated proliferation of HUVECs, and results showed that OD value of siFNIP1 group was significantly decreased compared with control group and siNC group (Fig. 3E). In agreement with these results, HUVEC migration was slowed down after treatment with siFNIP1 determined transwell assays test and scratch-wound healing assays (Fig. 3F–H). Additionally, downregulating FNIP1 also impaired tube formation of HUVECs (Fig. 3I–K). Together, these findings suggested that FNIP1 regulated angiogenesis of HUVECs and downregulating of FNIP1 in HUVECs resulted in impairment of angiogenesis.

2.4. Overexpression of FNIP1 rescued impaired angiogenesis of high-glucose-induced HUVECs

To verify whether FNIP1 rescued impaired angiogenesis of high-glucose-induced HUVECs, we overexpressed FNIP1 and then evaluated proliferation, migration, and tube formation capabilities of treated HUVECs in high glucose medium. Firstly, overexpressing of FNIP1 in HUVECs promoted expression of cell cycle-related mRNAs and proteins (Fig. 4A and B), fueling cell entry to the S stage (Fig. 4C and D). Then, CCK8 tests showed that OD value of FNIP1 group was significantly increased compared with high glucose group and the NC group (Fig. 4E). In agreement with these results, HUVEC migration was accelerated after overexpressing of FNIP1 (Fig. 4F–H). Additionally, overexpressing of FNIP1 also rescued impaired tube formation of HUVECs in high glucose medium (Fig. 4I–K). Together, these findings suggested that over-expressing of FNIP1 rescued impaired angiogenesis of HUVECs in high glucose medium.

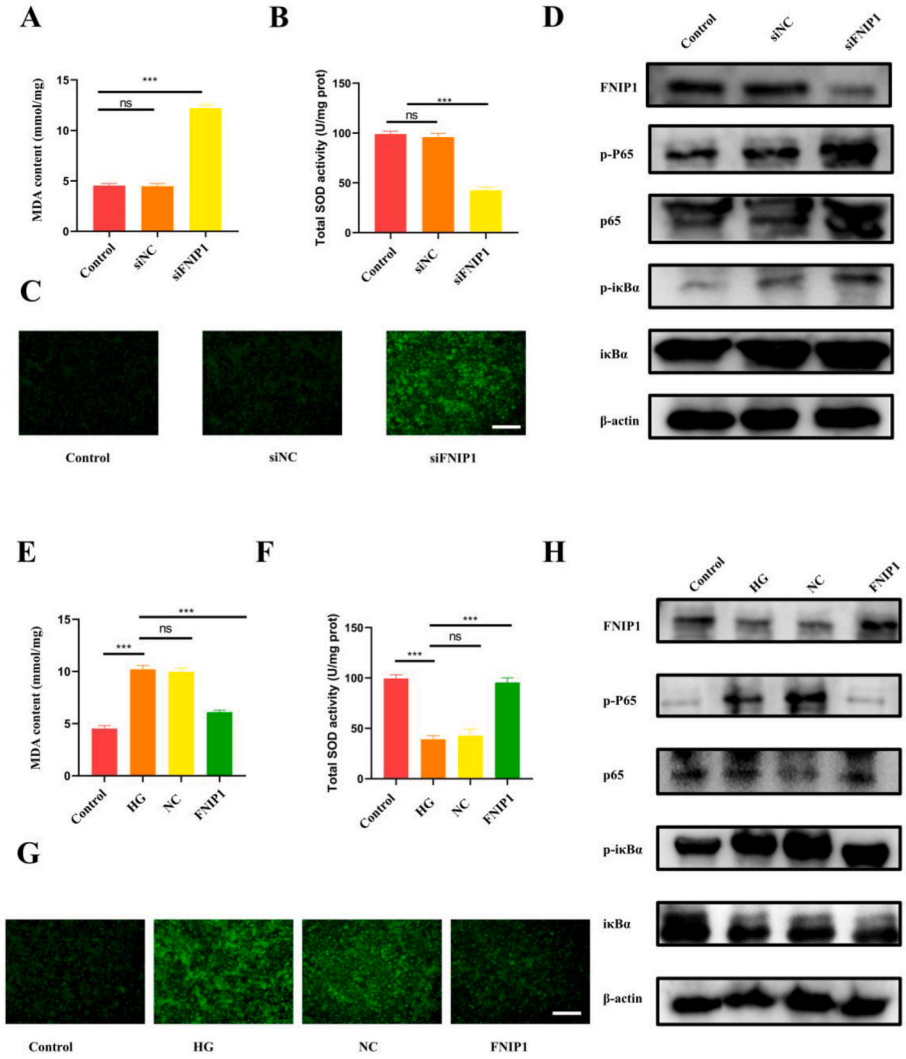

Fig. 2. FNIP1 participated in antioxidant defenses of HUVECs. (A), MDA levels of different treatments groups (Control, siNC, siFNIP1) were detected by thiobarbituric acid reaction. (B) SOD activities of different treatments (Control, siNC, siFNIP1) groups were detected by WST-8 assay. (C) ROS in HUVECs assessed with the DCFH-DA probe following different treatments (Control, siNC, siFNIP1), scale bar = 100 μm. (D) NFκB pathway proteins of different treatments groups (Control, siNC, siFNIP1) were detected by western blotting. (E) MDA levels of different treatments groups (Control, siNC, siFNIP1) were detected by thiobarbituric acid reaction. (F) SOD activities of different treatments (Control, HG, HG + NC, HG + FNIP1) groups were detected by WST-8 assay. (G) ROS in HUVECs assessed with the DCFH-DA probe following different treatments (Control, HG, HG + NC, HG + FNIP1), scale bar = 200 μm. (H) NFκB pathway proteins of different treatments groups (Control, HG, HG + NC, HG + FNIP1) were detected by western blotting. Differences were measured by *t*-test, data presented as means ± SD; ns, non-significant, ****p < 0.0001, ***p < 0.001, **p < 0.01, *p < 0.05.

2.5. FEM1b-FNIP1 axis inhibitor EN106 rescued impaired angiogenesis of high-glucose-induced HUVECs

In order to achieve tissue engineering approach to regulates the expression of FNIP1, the effects of FNIP1 conditioning agent were explored. Nathaniel J. Henning et al. [22]. Reported a FEM1b-targeting cysteine-reactive covalent ligand, EN106, which disrupts recognition of the key reductive stress substrate of FEM1B, FNIP1. Therefore, we decided to clarify the effects of EN106 in oxidative stress and angiogenesis.

Firstly, CCK8 tests were performed to figure out the appropriate concentration for cell culturing (Fig. S1). Results showed that EN106 promoted cell production significantly at 1 μM. Therefore, we decided to conduct subsequent experiments using 1 μM EN106. Then, the effects of EN106 in antioxidant defenses of HUVECs were tested. The MDA content was significantly decreased in the EN106 treating (FNIP1) group compared with high glucose group and the control group (Figs. S2 and A). The SOD activity was significantly increased in EN106 group (Figs. S2 and B). And fluorescence intensity of ROS was significantly decreased in EN106 group (Figs. S2 and C). Western blotting showed that EN106 downregulated the activation of NFκB signalling pathway (Figs. S2 and D).

Then, we clarified the effects of EN106 in angiogenesis. Applying of EN106 in HUVECs promoted expression of cell cycle-related mRNAs and proteins (Fig. 5A and B), fueling cell entry to the S stage (Fig. 5C and D). CCK8 tests showed that OD value of EN106 group was significantly increased compared with high glucose group and the control group (Fig. 5E). Then, transwell assays test and scratch-wound healing assays showed that HUVEC migration was accelerated after treating with EN106 (Fig. 5F–H). Additionally, treating with EN106 also rescued impaired tube formation of HUVECs in high glucose medium (Fig. 5I–K). In summary, these findings suggested that treating with EN106 reduced oxidative stress and rescued impaired angiogenesis of HUVECs in high glucose medium through the regulating of FNIP1.

2.6. HA-PBA-FA/EN106 hydrogel preparation and characterization

To regulate FNIP1 protein level and ameliorate oxidative stress, a novel glucose responsive hydrogel loading EN106 was designed. Before forming the hydrogel, we successfully synthesized phenylboronic acid-grafted HA (HA-PBA), which showed glucose responsive based on the bond of phenylboronate ester. Then, fulvic acid (FA) was added to serve as a crosslinking agent with inhibitor EN106 loaded to upregulate the protein level of FNIP1 (Schematic diagram 1).

To examine interactions between HA-PBA and FA, we performed FT-IR analysis of composite material. The results of the FT-IR spectra of the pure HA-PBA, FA and HA-PBA-FA composite material with various irradiation doses are presented in Fig. 6A. In the spectrum of HA-PBA, the absorption peak of HA-PBA at 1371.26 cm^{-1} was attributed to the B–O bond, indicating that phenylboric acid had been successfully

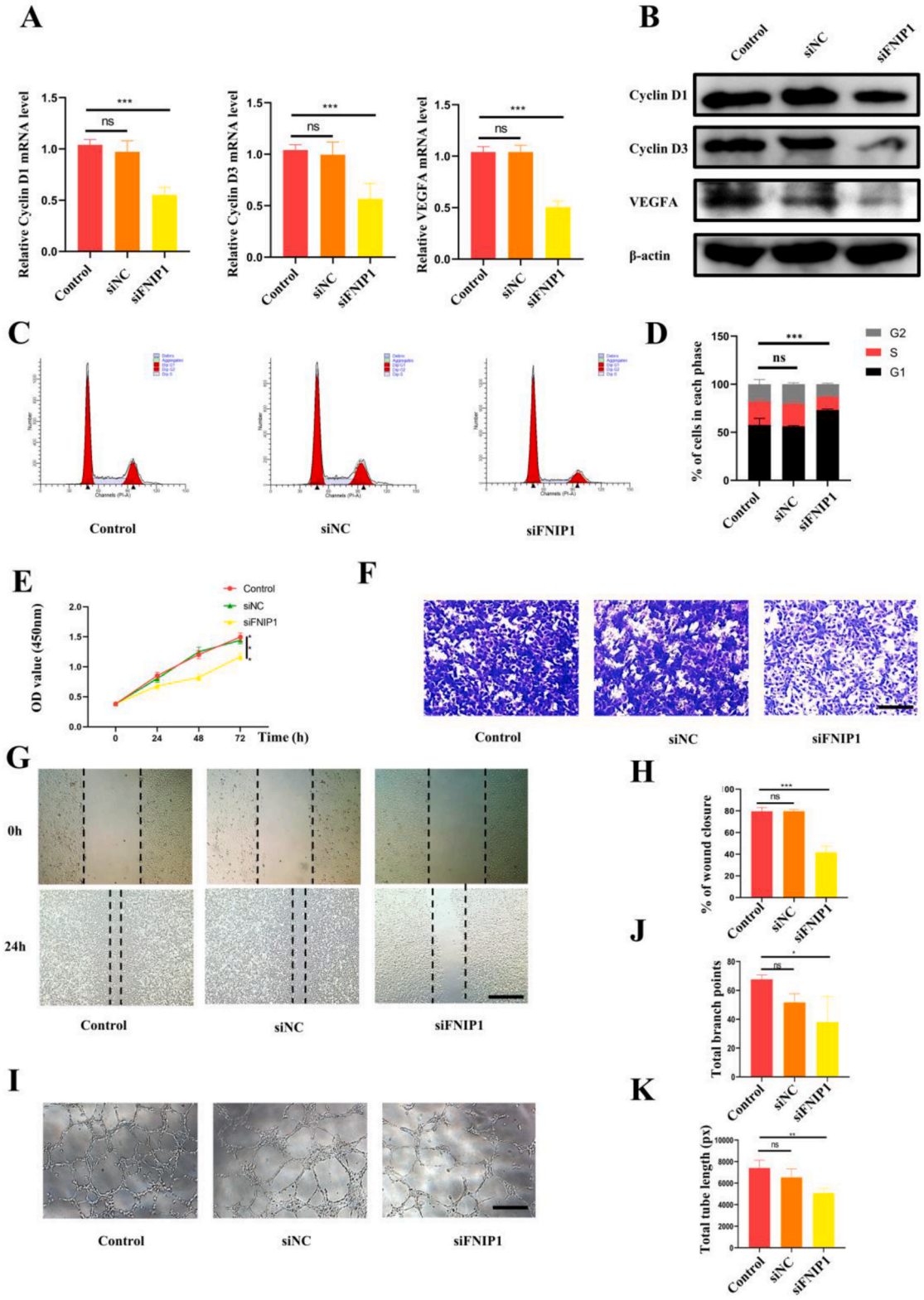

Fig. 3. Downregulation of FNIP1 inhibited angiogenesis of HUVECs (A) and (B) The effect of FNIP1 downregulation on the proliferation related protein Cyclin D1 and Cyclin D3 levels as well as VEGFA assessed by qRT-PCR analysis and western blotting. (C) and (D) Flow cytometry was applied to quantify cell cycle distribution. (E) Effect of FNIP1 downregulation on HUVECs' proliferation measured by CCK-8. (F) A transwell assay was used to assess the effect of FNIP1 downregulation on the cell migration of HUVECs. Scale bar = 50 μm. (G) In vitro wound healing assay of the HUVECs. Scale bar = 200 μm. (H) Quantitative analysis of the rate of wound closure at 24 h in the three groups. (I) Effects of FNIP1 downregulation on the tube formation ability of HUVECs. Scale bar = 200 μm. (J) and (K) Tube length and total branch points were quantified using ImageJ software. Differences were measured by *t*-test, data presented as means ± SD; ns, non-significant, ****p < 0.0001, ***p < 0.001, **p < 0.01, *p < 0.05.

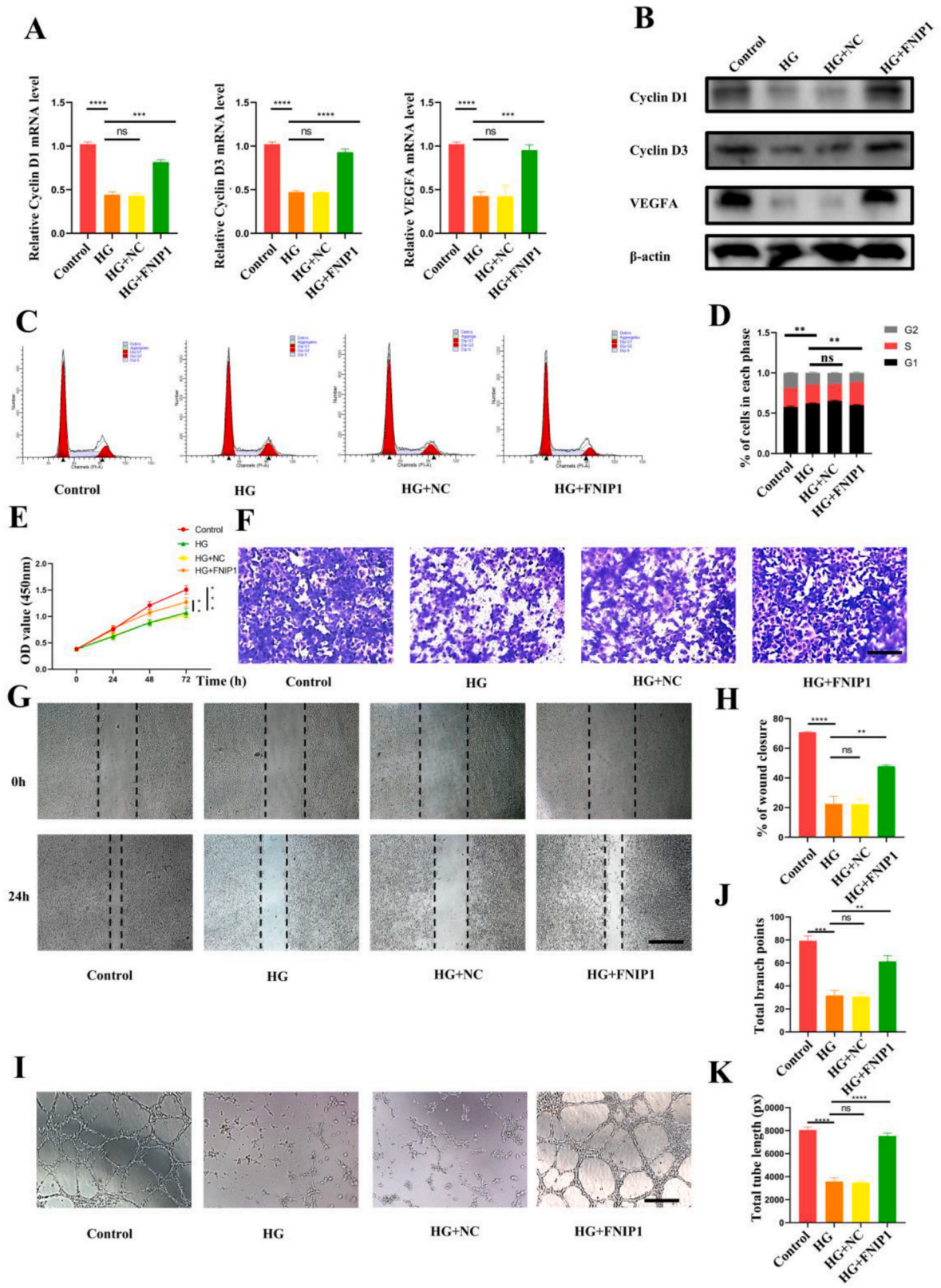

Fig. 4. Overexpression of FNIP1 rescued impaired angiogenesis of high-glucose-induced HUVECs (A) and (B) The effect of FNIP1 overexpression on the proliferation related protein Cyclin D1 and Cyclin D3 levels as well as VEGFA assessed by qRT-PCR analysis and western blotting. (C) and (D) Flow cytometry was applied to quantify cell cycle distribution. (E) Effect of FNIP1 overexpression on HUVECs' proliferation measured by CCK-8. (F) A transwell assay was used to assess the effect of FNIP1 overexpression on the cell migration of HUVECs. Scale bar = 50 μm. (G) In vitro wound healing assay of the HUVECs. Scale bar = 200 μm. (H) Quantitative analysis of the rate of wound closure at 24 h in the three groups. (I) Effects of FNIP1 overexpression on the tube formation ability of HUVECs. Scale bar = 200 μm. (J) and (K) Tube length and total branch points were quantified using ImageJ software. Differences were measured by *t*-test, data presented as means ± SD; ns, non-significant, ****p < 0.0001, ***p < 0.001, **p < 0.01, *p < 0.05.

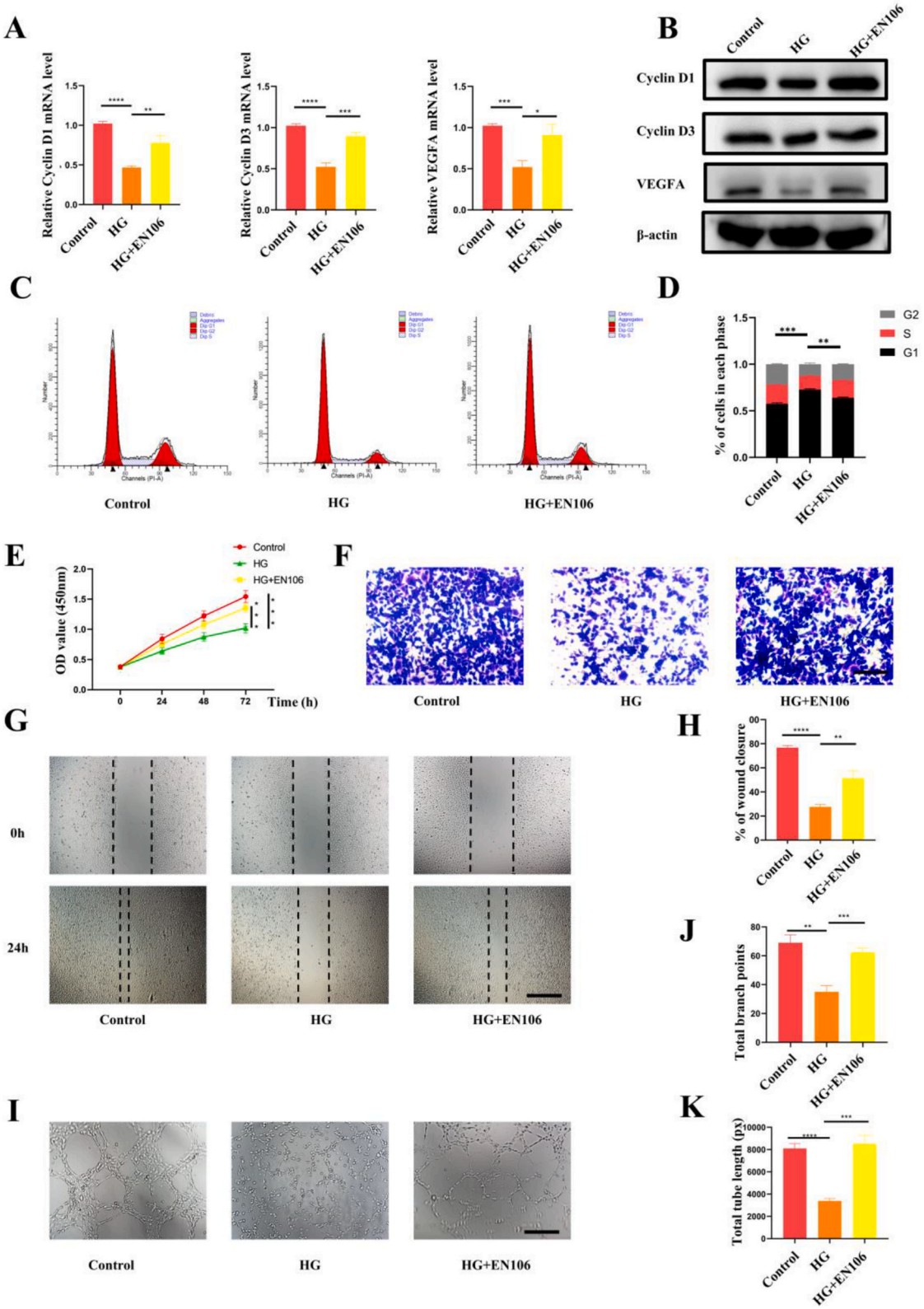

Fig. 5. FEM1b-FNIP1 axis inhibitor EN106 rescued impaired angiogenesis of high-glucose-induced HUVECs (A) and (B) The effect of EN106 on the proliferation related protein Cyclin D1 and Cyclin D3 levels as well as VEGFA assessed by qRT-PCR analysis and western blotting. (C) and (D) Flow cytometry was applied to quantify cell cycle distribution. (E) Effect of EN106 on HUVECs' proliferation measured by CCK-8. (F) A transwell assay was used to assess the effect of EN106 on the cell migration of HUVECs. Scale bar = 50 μm. (G) In vitro wound healing assay of the HUVECs. Scale bar = 200 μm. (H) Quantitative analysis of the rate of wound closure at 24 h in the three groups. (I) Effects of EN106 on the tube formation ability of HUVECs. Scale bar = 200 μm. (J) and (K) Tube length and total branch points were quantified using ImageJ software. Differences were measured by *t*-test, data presented as means ± SD; ns, non-significant, ****$p < 0.0001$, ***$p < 0.001$, **$p < 0.01$, *$p < 0.05$.

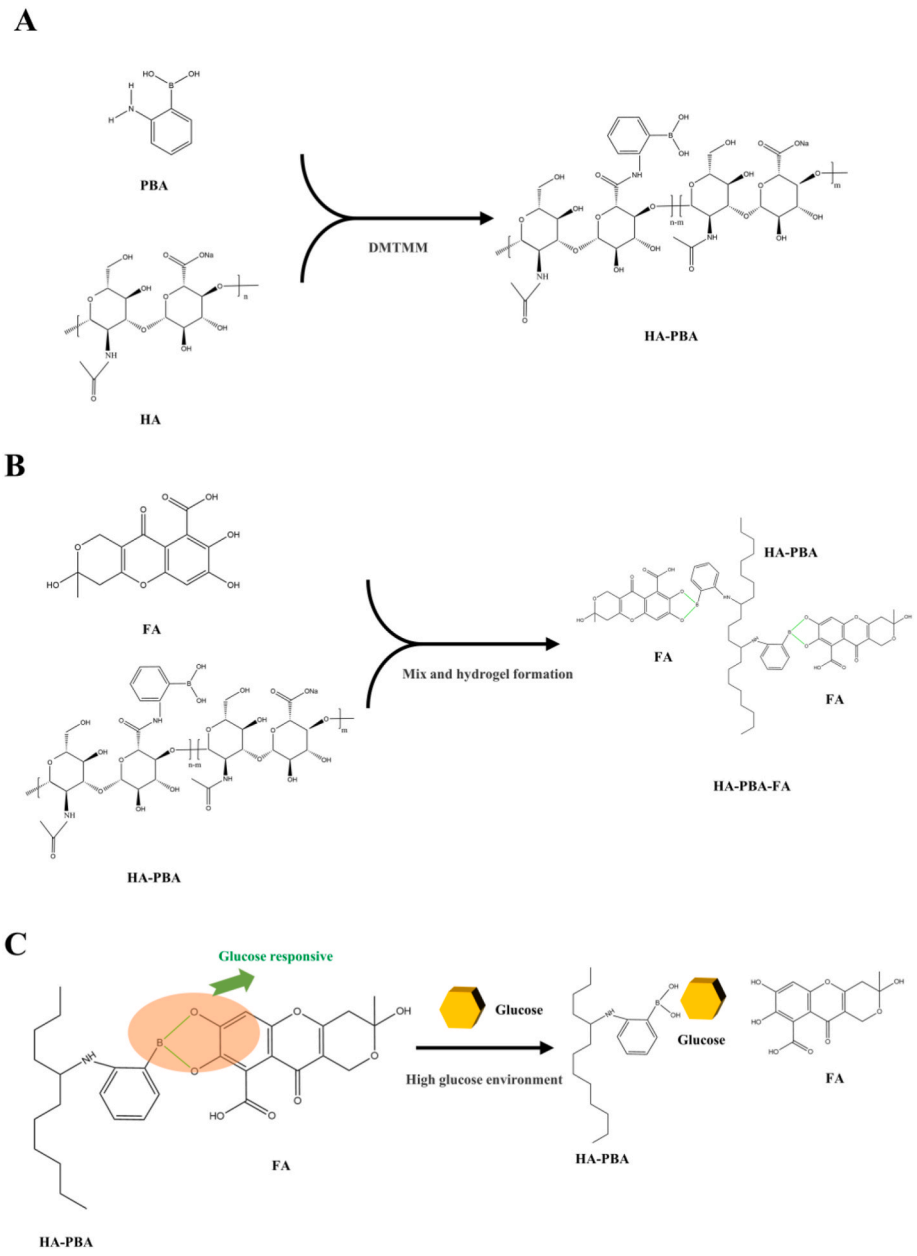

Schematic diagram 1. Preparation, structure and glucose responsive mechanism of HA-PBA-FA hydrogel. (A) Synthesis of hyaluronic acid phenylboronic acid polymer conjugates. (B) Fabrication of HA-PBA-FA hydrogel. (C) The dynamic phenylboronate ester structure between HA and PBA makes the hydrogel glucose responsive ability.

grafted onto hyaluronic acid. In the spectrum of pure FA, the presence of a C–O bond on phenyl ether was shown by the peak at 1153.09 cm^{-1}. In the spectrum of HA-PBA-FA, the absorption peaks at 1370.52 cm^{-1} and 1148.82 cm^{-1} due to the existence of the B–O bond and C–O bond on phenyl ether, suggesting that grafting and cross-linking reaction took place between HA-PBA and FA. Energy-dispersive X-ray spectroscopy (EDS) was performed to confirm the elements of HA-PBA-FA hydrogels (Fig. S3).

The creation of porosity in hydrogels has been considered an important process, which plays multiple roles of enhancing the total water sorption capability and the rate of response by reducing the transport resistance [23]. The surface morphology of HA-PBA-FA hydrogel was investigated by scanning electron microscope (SEM) and it was revealed in Fig. 6B. The presence of a continuous porosity network indicated the excellent water sorption capacity of the HA-PBA-FA hydrogel.

To test the mechanical properties of the hydrogels. We performed the rheological time sweep and the cycle loading–unloading compressive tests. The rheological time sweep results in Fig. 6C showed that the storage modulus (G′) is higher than loss modulus (G″) for all hydrogels, demonstrating the elastic characteristic of the hydrogels. Besides, the loading of EN106 not affect the mechanical properties of the HA-PBA-FA hydrogel. Then, the cycle loading–unloading compressive tests were conducted to evaluate the resistance of the hydrogels in the compression process. Fig. 6D showed that HA-PBA-FA hydrogel behaved a certain compressive strength and the loading of EN106 not affect the mechanical properties of the HA-PBA-FA hydrogel.

The excellent water absorption ability of hydrogel makes it possible to maintain the moist environment of the wound, which is crucial for better epidermal tissue repair. To test the water absorption ability of hydrogel, we performed swelling ratio test. Fig. 6E showed the equilibrium swelling ratio of hydrogels. Overall, all hydrogels can absorb

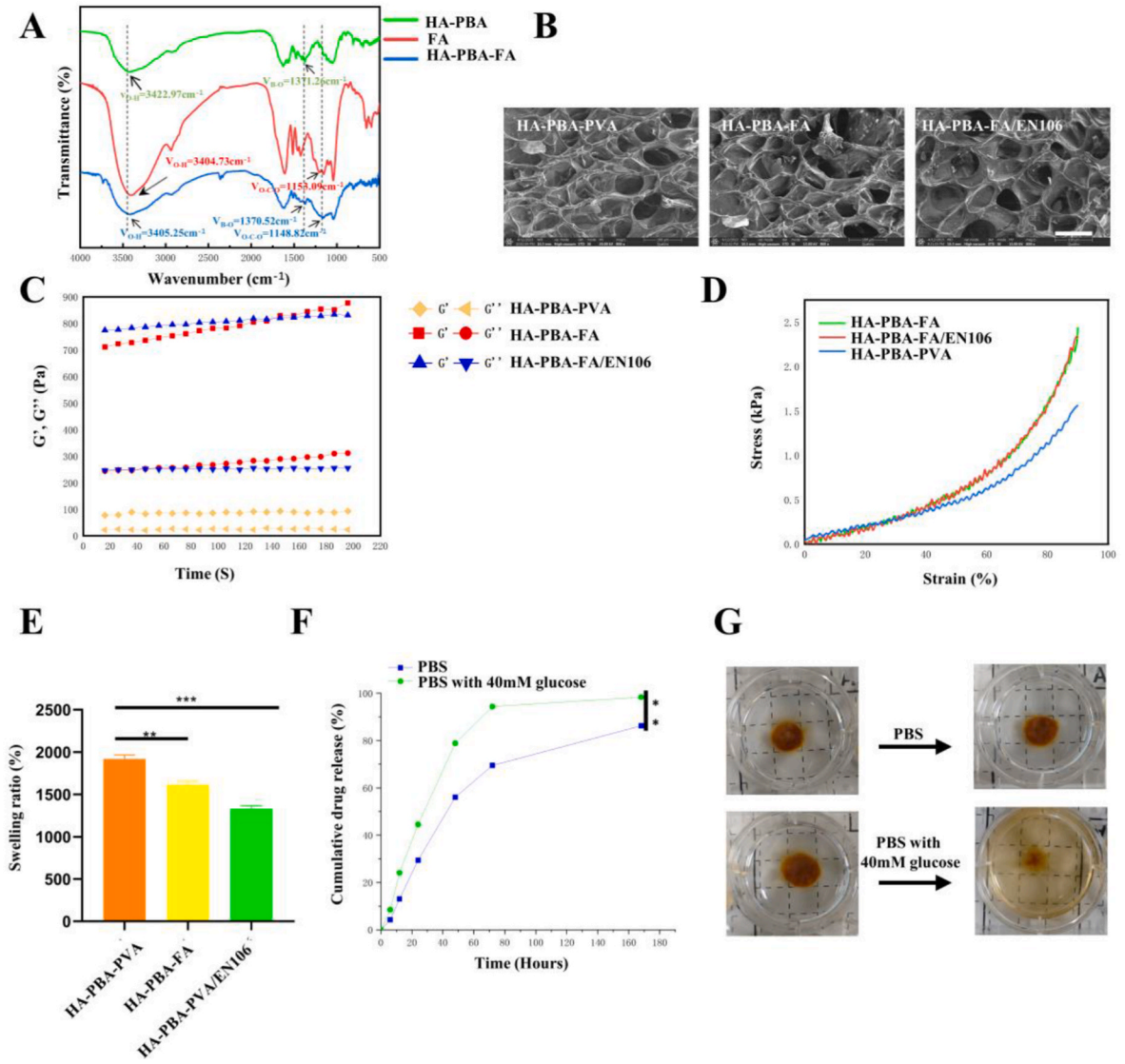

Fig. 6. Characterization of the HA-PBA-FA/EN106 hydrogel dressing. (A)FT-IR spectra for HA-PBA, FA and HA-PBA-FA. (B) SEM of HA-PBA-PVA hydrogel, HA-PBA-FA hydrogel, HA-PBA-FA/EN106 hydrogel. Scale bar = 100 nm. (C) The rheological time sweep curves of HA-PBA-PVA hydrogel, HA-PBA-FA hydrogel, HA-PBA-FA/EN106 hydrogel. (D) Compress strain–stress curves of HA-PBA-PVA hydrogel, HA-PBA-FA hydrogel, HA-PBA-FA/EN106 hydrogel. (E) Swelling ratio of HA-PBA-PVA hydrogel, HA-PBA-FA hydrogel, HA-PBA-FA/EN106 hydrogel. (F) and (G) Glucose responsive EN106 release of HA-PBA-FA/EN106 hydrogel. n = 3, differences were measured by *t*-test, data presented as means ± SD; ns, non-significant, ****p < 0.0001, ***p < 0.001, **p < 0.01, *p < 0.05.

more than 10 times their own mass of water. Specifically, HA-PBA-FA/EN106 hydrogel has the lowest swelling ratio of about 1339.6 ± 21.8% in all hydrogels, which also confirmed the cross-linking between HA-PBA and FA hydrogel network.

Theoretically speaking, the 1,2-diol structure in glucose can compete for the combination between catechol and phenylboronic acid, which makes the network of HA-PBA-FA hydrogel partially dissociated, thereby increasing the release of EN106 loaded in HA-PBA-FA/EN106 hydrogel. To test the glucose responsive release of EN106, we performed a drug release test. It can also be seen from Fig. 6F, that the final cumulative release of EN106 was 17.5% higher than that of the group without glucose.

Overall, the above test demonstrated the glucose responsive EN106 release of HA-PBA-FA/EN106 hydrogel, making it an advantage in the treatment of diabetic foot wounds.

2.7. Antibacterial and hemostatic abilities of the HA-PBA-FA/EN106 hydrogel

Antibacterial and hemostatic abilities are widely used to evaluate the goodness of hydrogel to sever as wound healing dress. To test the antibacterial ability of the HA-PBA-FA/EN106 hydrogel, *Staphylococcus aureus* (SA), and *Escherichia coli* (EC) were used. The results indicated that the HA-PBA-FA hydrogel exhibited robust antibacterial activity against all two bacteria, compared to phosphate-buffered saline (PBS) group. Furthermore, loading of inhibitor EN106 did not affect the antibacterial ability of hydrogel (Fig. 7A and B). To test the hemostatic ability of the HA-PBA-FA/EN106 Hydrogel, we performed a mouse hemorrhage test (Fig. 7C). As shown in Fig. 7D and E significantly reduced blood loss was observed after treatment with the HA-PBA-FA/EN106 hydrogel, which may be attributed to its efficient self-healing and excellent bio-adhesion. Collectively, these properties indicated that the HA-PBA-FA/EN106 hydrogels can form a compact protective barrier in diabetic wound healing process.

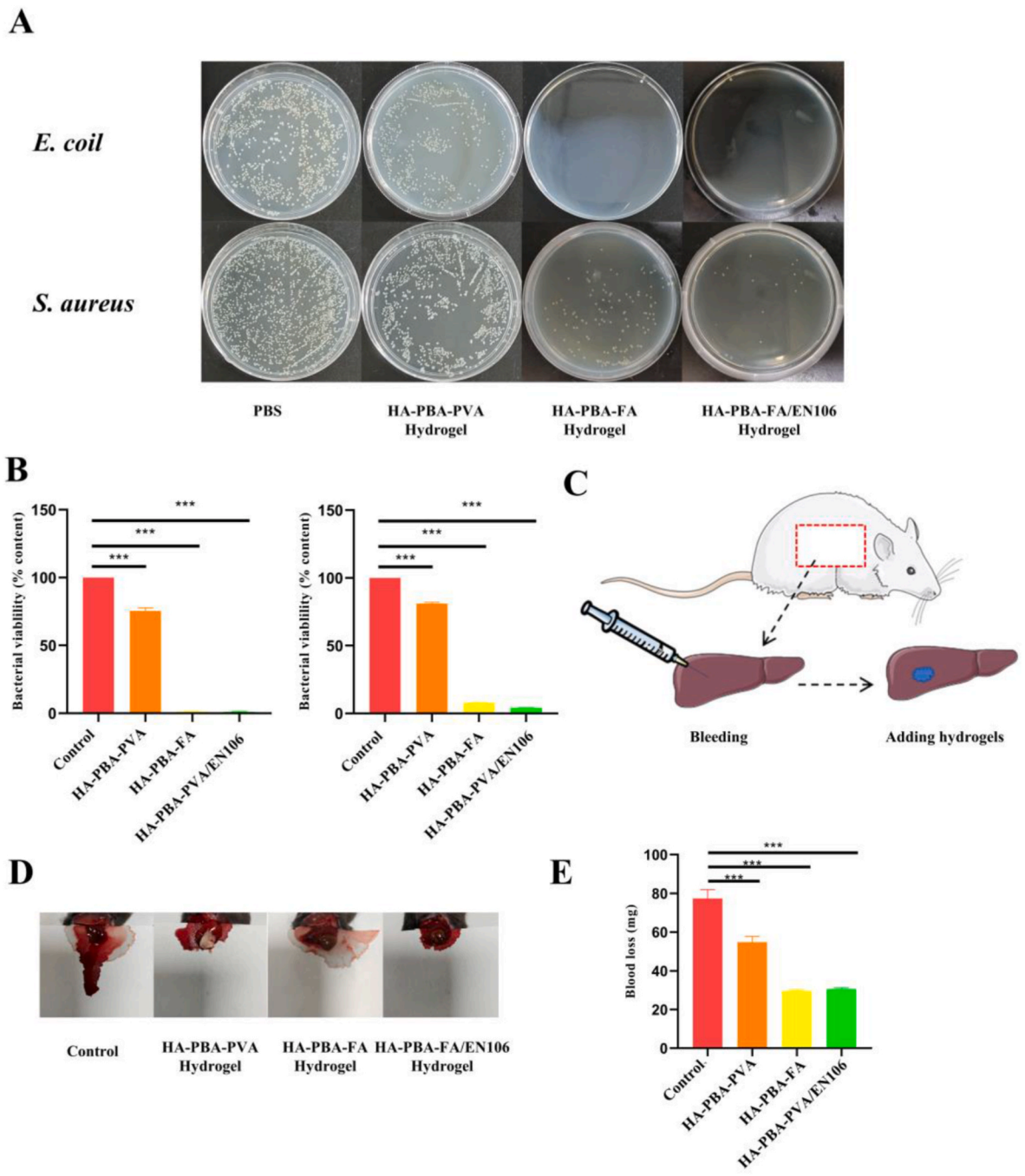

Fig. 7. Analysis of the antibacterial and hemostatic activities of the HA-PBA-FA/EN106 hydrogel dressing. (A) Clones and (B) viability of *E. coli*, *S. aureus*, after incubation for 12 h at 37 °C. (C) Schematic illustration of the mouse hemorrhagic liver model with the HA-PBA-FA/EN106 hydrogel dressing on the liver surface. (D) Photographs of livers treated with HA-PBA-PVA hydrogel, HA-PBA-FA hydrogel, HA-PBA-FA/EN106 hydrogel, and untreated (control) at 60 s. (E) Total amount of blood lost from the injured livers after 60 s of treatment with HA-PBA-PVA hydrogel, HA-PBA-FA hydrogel, HA-PBA-FA/EN106 hydrogel, and untreated (control). n = 3, differences were measured by *t*-test, data presented as means ± SD; ns, non-significant, ****p < 0.0001, ***p < 0.001, **p < 0.01, *p < 0.05.

2.8. HA-PBA-FA/EN106 hydrogel ameliorates ROS damage, induces M2 polarity, promotes angiogenesis and enhances cells survival in vitro

To address the ROS damage caused in hyperglycemic conditions, we included EN106 and fulvic acid (FA) in the hydrogel. The potential protection offered by our hydrogel against ROS in HUVECs was investigated under a cellular oxidative microenvironment induced by 40 mM glucose. HUVECs were co-incubated with hydrogel extract, and the results indicated that cells treated with the HA-PBA-FA/EN106 hydrogel extract had significantly reduced fluorescence in comparison with the controls. Therefore, the HA-PBA-FA/EN106 hydrogel was able to ameliorate oxidative stress effectively (Fig. 8A). Besides, we proved that HA-PBA-FA/EN106 hydrogel extract induced M2 polarity of RAW264.7 (Fig. 8B–E). Additionally, treating with HA-PBA-FA/EN106 hydrogel extract rescued impaired tube formation of HUVECs in high glucose medium (Fig. 8F–H). Furthermore, HUVECs viability was assessed by differential staining of live and dead cells. The measurement of the *in vitro* proliferation of HUVECs showed that cells incubated with the exact of HA-PBA-FA/EN106 hydrogel proliferated well over the 5-day duration of the experiment, with no significant differences between them and the controls (Fig. 8I).

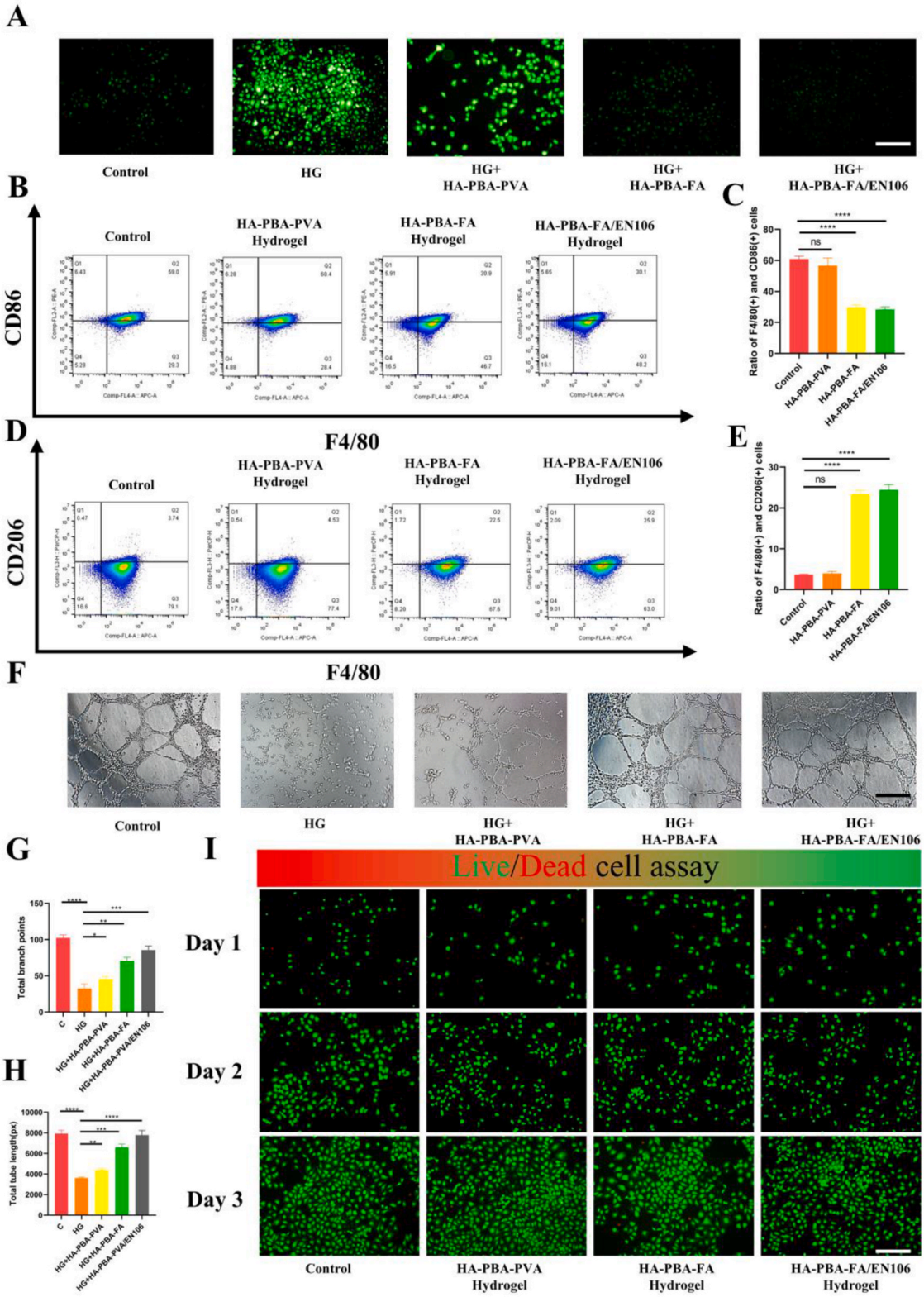

Fig. 8. HA-PBA-FA/EN106 hydrogel ameliorates ROS damage, induces M2 polarity of RAW264.7, promotes angiogenesis and enhances cells survival of HUVECs. (A) Reduction of ROS in HUVECs assessed with the DCFH-DA probe following different treatments. Green fluorescence: DCFH-DA indicates ROS level, scale bar = 100 μm (B-E) Flow cytometry analysis of polarity of RAW264.7 treated with exact of HA-PBA-PVA hydrogel, HA-PBA-FA hydrogel, HA-PBA-FA/EN106 hydrogel. (F) Effects of different treatments on the tube formation ability of HUVECs. Scale bar = 200 μm. (G, H) Tube length and total branch points were quantified using ImageJ software. (I)The *in vitro* proliferation of the HUVECs was measured by the proportions of live and dead cells (green fluorescence: Calcein-AM represents live cells; red fluorescence: PI represents dead cells.), scale bar = 100 μm Differences were measured by *t*-test, data presented as means ± SD; ns, non-significant, ****$p < 0.0001$, ***$p < 0.001$, **$p < 0.01$, *$p < 0.05$.

2.9. The HA-PBA-FA/EN106 hydrogel increased the wound closure rate, reduced inflammation, and promote collagen deposition in diabetic mice

To test whether the HA-PBA-FA/EN106 hydrogel could accelerate diabetic wound healing, a mouse model of chronic diabetic wounds was established and the effects of the hydrogel were assessed. As seen in Fig. 9A and B, the wound closure rate in the HA-PBA-FA/EN106 hydrogel group was higher than in the other groups. Tissue was collected from the five groups after euthanasia of the mice on day 7 and, day 21 post-injury, and H&E staining was performed, indicating that inflammation was reduced in the HA-PBA-FA hydrogel and the HA-PBA-FA/EN106 hydrogel groups. Wounds treated with the hydrogel showed a significantly higher thickness of granulation tissue formation than the control group, with the HA-PBA-FA/EN106 hydrogel group showing the highest degree of granulation tissue formation (Fig. 9C). Furthermore, Masson's trichrome staining showed that more extensive collagen deposition was seen in the HA-PBA-FA/EN106 hydrogel group, indicating that HA-PBA-FA/EN106 hydrogel have more superior ECM remodeling ability (Fig. 9D).

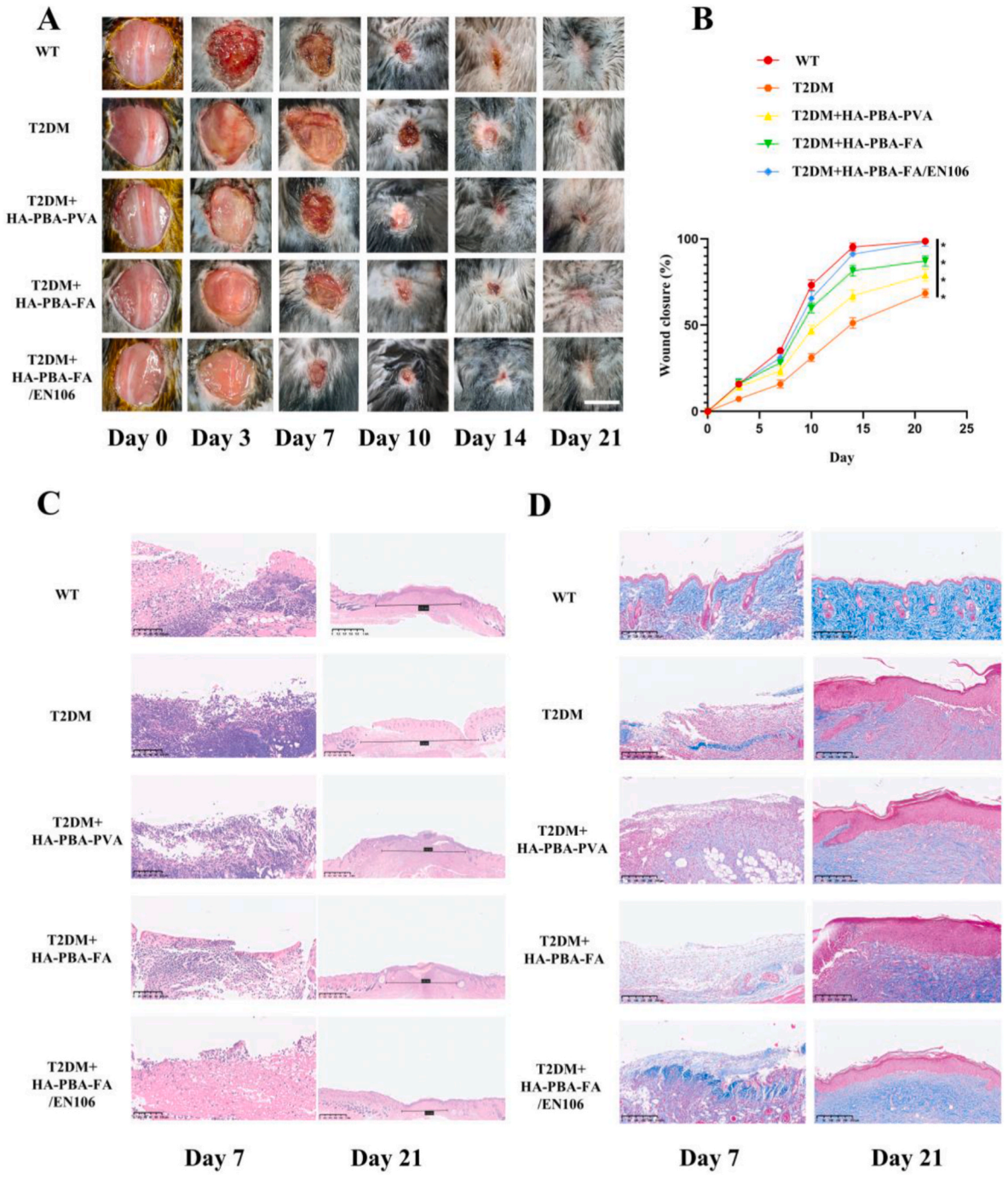

Fig. 9. The HA-PBA-FA/EN106 hydrogel increased the wound closure in diabetic mice. (A, B) Representative general images of the diabetic wounds in different treatment groups, and the statistical results of the wound closure ($n \geq 3$). (C, D) The hematoxylin and eosin (H&E) and Masson staining of the collected skin tissue at day 7 and day 21 post-wounding, Scale bar = 250 μm. Differences were measured by *t*-test, data presented as means ± SD; ns, non-significant, ****$p < 0.0001$, ***$p < 0.001$, **$p < 0.01$, *$p < 0.05$.

2.10. The HA-PBA-FA/EN106 hydrogel promoted angiogenesis and reduced the ROS level in diabetic mice

To investigate whether application of the HA-PBA-FA/EN106 hydrogel increased angiogenesis and reduced the ROS level in diabetic mice, we investigated blood perfusion and the presence of CD31 (+) cells in the diabetic wounds of different groups. As small animal Doppler examination performed to evaluate blood perfusion in the wound, a higher mean perfusion unit (MPU) ratio was found in the groups which were hydrogel-treated, with the HA-PBA-FA hydrogel group and the HA-PBA-FA/EN106 hydrogel group showing superior performance (Fig. 10A and B). Then, our data also showed that applying HA-PBA-FA/EN106 hydrogel in diabetic wounds increased expression of FNIP1 and VEGFA protein levels (Fig. 10C). Besides, greater numbers of CD31 (+) cells were visible in the hydrogen-treated wounds, indicative of enhanced angiogenesis. Moreover, the density of CD31 (+) cells was significantly higher in the wounds treated with the HA-PBA-FA and HA-PBA-FA/EN106 hydrogels compared to the other groups (Fig. 10D and E). To investigate whether application of the HA-PBA-FA/EN106 hydrogel reduced oxidative stress in diabetic wounds, we performed dihydroethidium (DHE) staining to detect intracellular ROS content *in vivo*. The application of the hydrogels resulted in a marked reduction in red fluorescence, with the HA-PBA-FA/EN106 hydrogel exhibiting the best ROS scavenging performance, indicating excellent antioxidative abilities (Fig. 10F–H). All these results indicated the noticeable pro-angiogenesis and antioxidant effect of the HA-PBA-FA/EN106 hydrogel in diabetic wound.

3. Discussion

Our results clarify the function of mitochondrial gatekeeper protein FNIP1 in antioxidant defenses of HUVECs, which significantly promoted angiogenesis and accelerated wound healing in mice. We also demonstrate that FEM1b-FNIP1 axis inhibitor EN106 can be embedded into a novel glucose responsive HA-PBA-FA hydrogel applied locally to the diabetic wound sites, providing a new potential for enhancing wound healing through its antioxidant and pro-angiogenesis effect.

Clinically, the wound healing of diabetic feet is often delayed due to the high glucose concentrations [24], so the glucose responsive release behavior of HA-PBA-FA/EN106 hydrogel can well promote the healing of high glucose concentration wounds. The rapid complexation between boronic acid and 1,2-diol or 1,3-diols leads to a dynamic boronic ester bond in aqueous solution under ambient conditions without any catalyst and has been studied and applied in many areas, including analyte sensors, disease diagnosis, and drug delivery [25]. Besides, boronic acid compounds normally show low toxicity, and engineered hydrogel networks based on boronic ester have been reported [26]. In this study, HA-PBA-FA/EN106 hydrogel behaves low cytotoxicity *in vitro* and glucose-responsive manner, making it possible to become a potential diabetic wound healing dress.

Furthermore, we showed that the HA-PBA-FA/EN106 hydrogel alleviated oxidative stress in diabetic wounds. The decreased oxidative stress was due to the regulation of FEM1b-FNIP1 axis. In the present study, the function of FNIP1 in antioxidant defenses was proved following with its conditioning agent EN106 incorporated into the HA-PBA-FA hydrogel to ameliorate the ROS damage in the diabetic wounds. It was shown that the HA-PBA-FA/EN106 hydrogel could efficiently eliminate ROS in HUVECs induced by high glucose medium. Compared to the control group, use of the HA-PBA-FA/EN106 hydrogel led to improved cellular proliferation, indicating that the EN106 was able to protect the endothelial cells from the oxidative microenvironment of the wound, which may have partially contributed to the enhanced diabetic wound healing observed in the HA-PBA-FA/EN106 hydrogel group compared to the control group. The decreased oxidative stress may also be associated with decreased activation of NFκB signalling pathway. NFκB signalling pathway shows functional links with inflammatory and oxidative stress [27,28], and NFκB is one of the crucial molecules contributing to end-organ damage T2DM [29].

Successful wound healing is dependent on angiogenesis [30]. In normal wound healing process, endothelial cells proliferate, migrate, and branch to form new blood vessels in the wound sites, allowing re-supply of oxygen and other nutrients [31]. In diabetic wound healing, studies have summarized many compromising factors for angiogenesis such as the loss of heparan sulfate proteoglycans, alterations in inflammatory response, increased proteolysis and alterations in ROS signaling [32]. Based on abovementioned theories, we tested the effects of FNIP1 and subsequent HA-PBA-FA/EN106 hydrogel on angiogenesis. We found that upregulated FNIP1 protein level increased HUVECs survival and tube formation *in vitro*. In diabetic wounds, applying HA-PBA-FA/EN106 hydrogel significantly upregulated VEGFa protein level and increased CD31 (+) cells. The quicker angiogenesis may also be attributed to the reduction of inflammatory and oxidative stress.

Taken together, the rapid wound healing in the present study, was likely due to a multifaceted action of the HA-PBA-FA/EN106 hydrogel dressing, including the glucose-responsive release of EN106. The HA-PBA-FA/EN106 hydrogel dressing could absorb wound exudate, maintain moisture, and produce a favorable environment for wound healing with low levels of ROS. The antibacterial and ROS-dissipative actions of the HA-PBA-FA/EN106 hydrogel dressing could protect the wound against both bacterial infection and ROS damage while the glucose responsive release of EN106 promoted angiogenesis and wound healing.

4. Conclusion

The present study introduces a novel application of glucose responsive HA-PBA-FA/EN106 hydrogel as an antioxidant therapy for diabetic wound healing. Firstly, our findings provide the information of FNIP1-based antioxidant defenses of HUVECs and subsequent enhancement of angiogenesis and wound healing. Then we explore the tissue engineering approach to regulate FNIP1 and promote diabetic wound healing by introducing glucose responsive HA-PBA-FA/EN106 hydrogel. The HA-PBA-FA hydrogel dressing provides bio-adhesive properties and fulvic acid to avoid the negative effects of the external environment and provides comprehensive long-term antibacterial protection for the diabetic wound. The dynamic phenylboronate ester structure makes it possible to degrade and release drugs in a glucose response manner. Integrating glucose responsive release of EN106, our HA-PBA-FA hydrogel synergistically ameliorated oxidative stress, induced angiogenesis, enhanced proliferation, and collagen accumulation, thus demonstrating significant potential for promoting diabetic wound healing *in vivo*. In summary, our glucose responsive HA-PBA-FA/EN106 hydrogel represents a versatile treatment for preventing infection, ameliorating oxidative stress, and promoting angiogenesis in diabetic wound healing.

5. Materials and methods

5.1. Synthesis of hyaluronic acid phenylboronic acid polymer conjugates (HA-PBA)

400 mg (1 mmol) of hyaluronic acid (HA, aladdin) were added in 80 mL de-ionized (DI) water under constant stirring. After dissolving completely, 188 mg (1 mmol) phenylboronic acid (PBA, aladdin) and 320 mg (1 mmol) 4-(4,6-dimethoxy-1,3,5-triazin-2-yl)-4-methyl-morpholinium chloride (DMTMM, aladdin) were added to the HA solution separately. After all the agents were dissolved, add 1 M HCl solution to adjust the pH of the solution to 6.5 using. At the same time, another reaction was performed using 1 mmol HA, 1 mmol PBA, and 2 mmol DMTMM at the same pH. Then, all reaction mixtures were stirred at room temperature for 72 h. After that, the mixtures were transferred to 6–8 kDa molecular weight cut-off (MWCO) dialysis bags (Spectrum) and dialyzed against DI water for at least 4 days at room temperature.

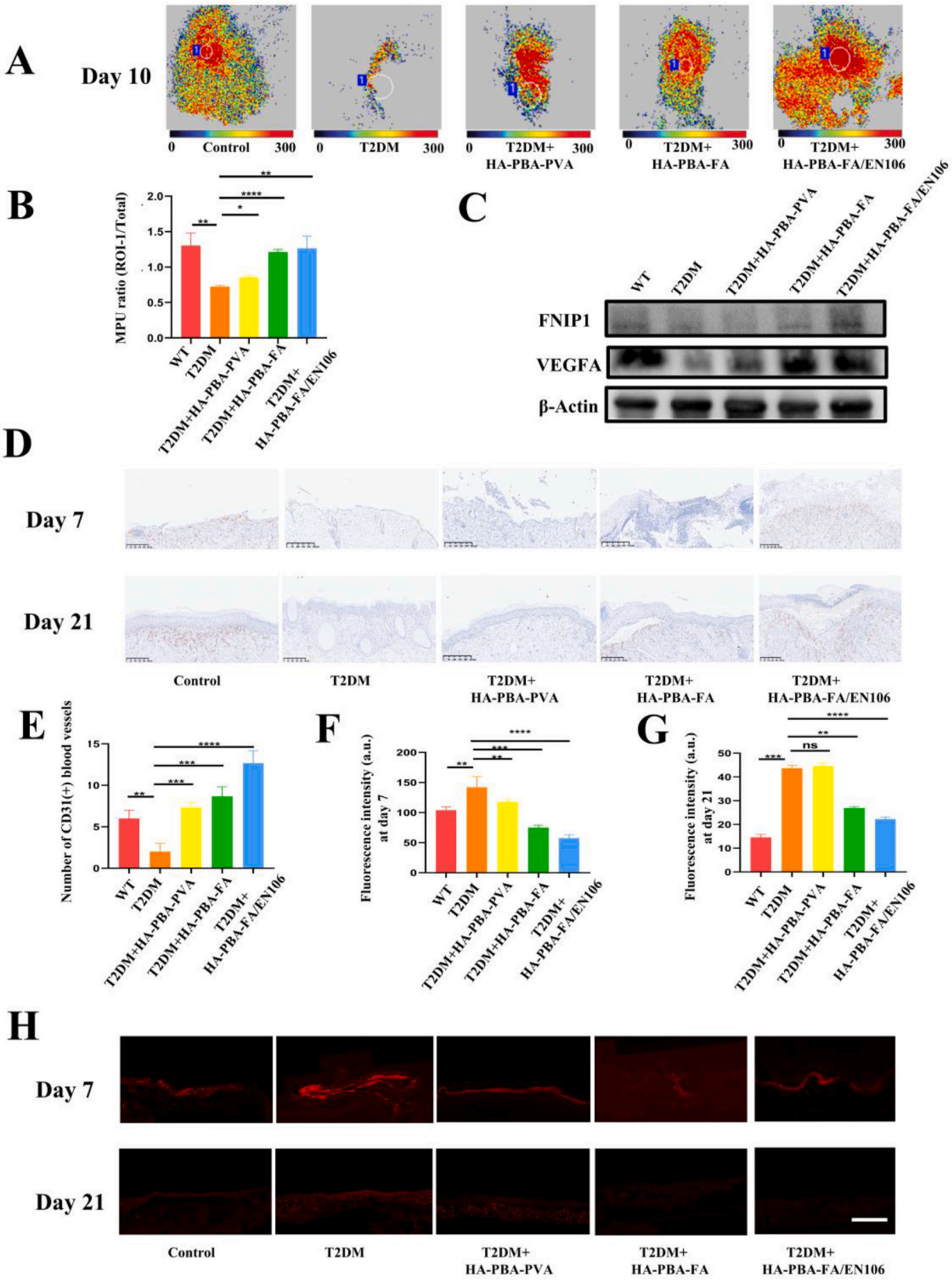

Fig. 10. The HA-PBA-FA/EN106 hydrogel promoted angiogenesis and reduced the ROS level in diabetic mice. (A, B) Wounds were created in a diabetic mouse model and divided into five groups according to the different treatments. At day 10 post-wounding, the blood perfusions among the five groups were detected by small animal doppler examination. (C) Western blotting results of FNIP1 and VEGFA expression in the skins of five groups at day 10 post-wounding. (D) Representative immunohistochemical analysis images of CD31, Scale bar = 250 μm. (E) Quantification of the number of CD31 positive among the different groups using the ImageJ software. (F–H) Levels of ROS in wound area measured by dihydroethidium (DHE) following different treatments, Scale bar = 50 μm. Differences were measured by *t*-test, data presented as means ± SD; ns, non-significant, ****$p < 0.0001$, ***$p < 0.001$, **$p < 0.01$, *$p < 0.05$.

Change water twice every day during the process. The dialyzed solutions were freeze-dried using a benchtop lyophilizer (model FreeZone, Labconco) for 72 h to obtain the HA-PBA polymer conjugates. The conjugates were stored in a desiccator at room temperature before use.

5.2. Fabrication of HA-PBA-FA and HA-PBA-PVA hydrogel

HA-PBA-FA hydrogel was prepared by mixing 10% HA-PBA, dissolved in phosphate buffer (PBS) at pH 7.4, with corresponding 10% FA, dissolved in PBS at pH 7.4, in a 9:1 vol ratio at room temperature. The HA-PBA-PVA hydrogel was prepared in a similar way by mixing 10 wt% HA-PBA and 10% PVA in a 9:1 vol ratio, respectively.

5.3. Morphology characterization

The prepared hydrogel was rapidly freeze with liquid nitrogen to fix its morphology before lyophilization. A scanning electron microscope (SEM) was used to cross section the hydrogel after uniform gold spraying. The distribution of the FA in the composite hydrogel was observed through energy-dispersive X-ray spectroscopy (EDS).

5.4. Fourier transform infrared spectroscopy (FT-IR)

Firstly, mix the samples with potassium bromide in the ratio of 1:100 and pelleted. Then the spectra were recorded using NICOLET 380 FTIR spectrometer operating in the spectral range of 4000–500 cm^{-1} with the resolution of 1 cm−1 in transmission mod.

5.5. Swelling ratio test

The swelling ratios of the developed hydrogel (n = 3) were determined gravimetrically. The prepared HA-FA hydrogels were immersed in PBS (pH 7.2) for 24 h. After wiping with filter paper to remove excess liquid on the sample surface, the swelled hydrogels were collected to be weighted and the weight was recorded as Ws. Then, the collected hydrogel samples were dried in a dryer for 24 h and weighed again and the weight was recorded as Wd. The swelling ratios were calculated using the following equation: Swelling ratio (%) = (Ws − Wd)/Wd × 100.

5.6. In vitro glucose response degradation of HA-PBA-PVA hydrogels

For EN106 (TargetMol), its release from the HA-PBA-FA hydrogels was carried out in a PBS buffer and 40 mM glucose PBS buffer at room temperature. EN106 was preloaded into the hydrogel samples according to the following protocol: 2 μl EN106 solution (0.2 mM) was directly mixed with 180 μl 10 wt% HA-PBA first, and then mixed with 20 μl 10% FA solution to form drug loaded hydrogels. The drug loaded hydrogels were then placed inside small vials containing 10.0 mL PBS solution (one piece of hydrogel per vial). The vial was incubated at room temperature with a constant reciprocal shaking (ca. 100 rpm). The EN106 contents were then analyzed by high performance liquid chromatography (HPLC). The following are the details of measuring the EN106 concentration via HPLC. To determine the release amounts of the drug at predetermined time points, 50 μL of the immersion solution was removed from the vial and added into a HPLC vial followed by adding 950 μL PBS buffer to dilute the solution. The solution was thoroughly vortexed before tested by using a HPLC (HP 1100 model, Palo, Alto, CA, USA) equipped with a diode array detector. A C18 reversed phase column (5 μm, 4.6 × 250 nm, Alltech Adsorbosphere XL) was used as the stationary phase, while the mobile phase consisted of acetonitrile and water (pH 3.0) in the volume ratio of 63: 37. The injection volume was 50 or 100 μL based on the released EN106 concentration and the mobile phase was pumped at a flow rate of 2.0 mL min^{-1}. Detection was at 240 nm with a UV detector. The confirmation of the EN106 chemical structure was carried out by the GC-MS method and the major diagnostic MS fragments were analyzed.

5.7. Hemostasis test

The hemostatic potential of the HA-FA hydrogel was evaluated using a hemorrhaging liver mouse (Kunming mice, 30–35 g, male). The mouse was anesthetized with 10 ml/kg 4 wt% chloral hydrate (Sigma, USA) and anchored on a surgical cushion. The liver of the mouse was exposed by an abdominal incision. A pre-weighted filter paper placed on a paraffin film was positioned beneath the liver. The bleeding was induced in the liver using a 20 G needle with the cushion at about 30° angle, and the HA-FA hydrogel was immediately applied on the bleeding site. The weight of the filter paper with the absorbed blood was measured and compared with control group (no treatment after pricking the liver) 3 min later. All measurements were replicated three times.

5.8. Bioinformatics analysis and protein-protein interaction (PPI) network construction

The gene expression data were obtained from the Blueprint Consortium. A full list of the investigators who contributed to the generation of the data is available from www.blueprint-epigenome.eu. The protein-protein interaction (PPI) network of FNIP1 and the putative target were constructed utilizing the online tool NetworkAnalyst (https://string-db.org/).

5.9. HUVEC culture and transfection

HUVECs were incubated with RPMI 1640, which containing 10% FBS (Cyagen Biosciences, Wuhan). Lipofectamine 3000 was applied for cell transfection according to the instructions. HUVECs were cultured with 95% humidity and 5% CO2 at 37 °C. The FNIP1 plasmid and FNIP1 siRNA were constructs from Genechem (Shanghai). The FNIP1 siRNA were constructs from Tsingke Biotechnology (Wuhan). The cells expressing FNIP1 (HUVECFNIP1) was obtained by transfected with FNIP1 plasmid (Genechem, Shanghai). Likewise, FNIP1 in cells were detected (HUVECFNIP1−/−) by transfected with FNIP1 siRNA (Tsingke Biotechnology,Wuhan). The siRNA sequences of Human FNIP1 are as follows: Sense (5′-3′), GGUAGUUGGCAAACGACAA, antisense (5′-3′), UUGUCGUUUGCCAACUACC.

A large number of HUVECs were transfected with the FNIP1 plasmid or siRNA, and the cell RNA was collected within 48 h after successful transfection for the qRT-PCR and the cell protein was collected within 72 h after successful transfection for the Western Blotting.

5.10. qRT-PCR analysis

TRIzol® was applied to extract the total RNA from cells and callus. RNA was reversely transcribed into cDNA with HiScript III RT SuperMix (Vazyme, China), and quantified using 2x SYBR Green qPCR Mix. Relative mRNA expression folding alteration was calculated with the 2−ΔΔCt approach and the primer sequences are as follow:

Human FNIP1, forward, CCATTTCCTTCCCCAAACT, reverse, TTAGGGCCACAGCTTTCAT; Human β-actin, forward, CCACACTGTGCCCATCTAC, reverse, AGGATCTTCATGAGGTAGTCAGTC; human Cyclin D1, forward, TTGCCCTCTGTGCCACAGAT, reverse, TCAGGTTCAGGCCTTGCACT; human Cyclin D3,forward, CTGGCCATGAACTACCTGGA, reverse, CCAGCAAATCATGTGCAATC; human VEGFA, forward, CACCCACCCACATACATACAT, reverse, AGTCTCTCATCTCCTCCTCTT.

5.11. Western blot

The cell samples were lysed by buffer containing 1% protease and phosphatase inhibitor cocktail (NCM Biotech, Suzhou). The SDS-PAGE-separated protein samples were then transferred to NC membranes

(Millipore). Afterwards, NC membranes blocked with 5% skim milk for 1 h and then incubated at 4 °C overnight with homologous primary antibodies for FNIP1, Cylin D1, Cylin D3, VEGFA (Proteintech Group, Wuhan), NFκB-p65, IκBα,phosphorylated NFκB-p65, phosphorylated IκBα (ABclonal, Wuhan)and β-actin (Abcam, UK). Blots were incubated with secondary antibodies at 4 °C for 4 h, conjugated with horseradish peroxidase (HRP, Aspen). At the end, the proteins were observed by chemiluminescence examination system.

5.12. Transwell assays

A total of 5 × 104 HUVECs suspended in FBS-free medium were inoculated in the upper chambers of transwell 24-well plates (3422, Corning, USA). The lower chambers were filled with 600 μL of FBS-contained medium as nutritional attractants. After 24 h of culture, cells were washed in PBS three times, fixed in 4% paraformaldehyde for 30 min, and then stained with 0.5% crystal violet for 30 min. The non-invasive or non-migrated cells were removed using clean cotton swabs. Three visual fields for each well were randomly photographed under a bright field microscope.

5.13. Scratch-wound healing assays

HUVECs were inoculated into 6-well culture plates. A sterile 200-μL pipette tip was utilized to scratch the surface of cells at a confluence of 90–100%, in the shape of a cross. PBS was used to remove the floating cells. The scratches were photographed at 0 h, 12 h, 24 h and 36 h under an inverted microscope (IX53, Olympus, Japan).

5.14. Tube formation assay

HUVECs (2 × 104/well) were plated in 96-well plates pre-coated with Matrigel, incubated for 45 min, and then for a further 6 h. Three randomly-chosen fields were examined using an inverted microscope and the branch points and tube lengths were measured using ImageJ.

5.15. In vitro cytotoxicity

The Calcein-AM/PI double staining kit (Sigma-Aldrich) was applied to evaluate the viability of HUVECs cultured in RPMI 1640 with hydrogel extract liquid. Fluorescence images were acquired using a microscope (IX53, Olympus, Japan) at 24 h, 48 h and 72 h.

5.16. Flow cytometric analysis

All antibodies were obtained from eBioscience. Lineage-specific antibodies, F4/80 (#123107, Biolegend, San Diego, CA, USA) and CD 209 (#12-2092-80, Sigma Aldrich) and F4/80 and CD206 (#141705, Biolegend) and analyzed with FlowJo software (version: FlowJo v10.6.1). Staining with propidium iodide (PI) and Annexin V (using the eBioscience FITC/PI apoptosis detection kit) were used for the analysis of the cell cycle and apoptosis, respectively, following the manufacturers' directions and were evaluated by flow cytometry.

5.17. Generation of diabetic mice

The Institutional Animal Care and Use Committee of the Tongji Medical College, Huazhong University of Science and Technology approved all animal studies (IACUC Number: 2523). The diabetes model was established in male C57BL/6J mice (6-weeks-old) by feeding a high-fat diet for 4 weeks, followed by daily intraperitoneal administration of streptozotocin (STZ; 40 mg kg^{-1} day^{-1}) for 7 days. If the fasting blood glucose level was over 16.7 mmol L^{-1} for three successive measurements, the mice were considered to be diabetic and were used for the following experiments.

5.18. Murine wound model

The STZ-induced diabetic mice were anesthetized with intraperitoneal pentobarbital sodium (50 mg kg−1; Sigma Aldrich) 1.0 × 1.0 cm full-thickness excision skin wounds were made. The mice were randomly divided into groups that were injected with 200 μL of sample on days 0, 3, 5, 7, 10, and 14 after the establishment of the wound (n = 8). The wounds were covered with transparent dressings (Tegader TM Film) and were photographed and measured with a caliper on days 0, 3, 5, 7, 10,14 and 21. The degree of wound closure was determined by ImageJ as follows:

$$Cn = (A0 - An)/A0 \times 100\%$$

where Cn is the percentage reduction of the wound area on the respective days; A0 is the size of the original wound; An is the area of the wound on the respective day after the injury.

5.19. H&E and masson staining

Mouse skin wound tissues were fixed in 4% paraformaldehyde, embedded in paraffin, and cut into 4-μm-thick sections. The sections were stained with H&E or Masson's trichrome and imaged under a PANNORAMIC Flash series digital scanner (3DHISTECH, Hungary).

5.20. DHE staining

The intracellular ROS levels were assessed by staining with the ROS probe DHE (5 μm) for 10 min and washed three times with PBS. Images were obtained with the IX53 microscope.

5.21. IHC staining

The mice were sacrificed on day 14 and the wound tissues were embedded in paraffin and stained for CD31. Antigen retrieval was performed for 15 min in citrate buffer, followed by blocking for 30 min in goat serum. The samples were stained with anti-CD31 (1:100; Abcam, ab28364) antibodies overnight at 4 °C, washed in PBS and stained and counter-stained with DAB and hematoxylin, respectively. The sections were evaluated under a microscope (IX53, Olympus, Japan) to evaluate micro vascularization at the wound sites by counting the numbers of $CD31^+$ cells over five fields. Individual vessels were defined as those with diameters between 2 and 10 μm diameter.

5.22. Small animal Doppler

10 days after the operation, an LSCI (laser speckle contrast imaging) system was applied to examine local blood perfusion and a PSI-ZR PeriCam system (PERIMED Ltd, Stockholm, Sweden) was used to acquire images of the wounds. An invisible nearinfrared (NIR) laser at 785 nm was used to determine blood perfusion, expressed as perfusion units. The wounds were photographed at a constant distance and using the same dimensions for the area. The MPU ratio was determined using PIMSoft (Moor Instruments Ltd, Axminster, UK), expressed as the correlation of the MPU of the wound area (ROI-1) to the MPU of the region surrounding the wound (ROI-Total), using flux images of individual wound sites.

5.23. Statistical analysis

Data were displayed as mean ± standard deviation (SD). Statistical analysis was performed using Student's t-test (two groups) or ANOVA with Tukey's post hoc test (over two groups). Significance was considered when $p < 0.05$.

Data availability

All data of this study are available within the paper.

Ethic approval and consent to participate

The Institutional Animal Care and Use Committee of the Tongji Medical College, Huazhong University of Science and Technology approved all animal studies (IACUC Number: 2523).

CRediT authorship contribution statement

Wenqian Zhang: Conceptualization, Data curation, Writing – original draft. **Kangkang Zha:** Investigation, Data curation, Writing – original draft. **Yuan Xiong:** Data curation, Writing – original draft. **Weixian Hu:** Investigation, Resources. **Lang Chen:** Investigation, Formal analysis. **Ze Lin:** Visualization. **Chenyan Yu:** Technical assistance and made critical contributions to the, Conceptualization, Writing – original draft, revised the manuscript. **Wu Zhou:** Revised the manuscript. **Faqi Cao:** Visualization. **Hankun Hu:** Supervision, Validation. **Bobin Mi:** Conception, revised the manuscript. **Guohui Liu:** Conception, Supervision, Writing – original draft.

Declaration of competing interest

The authors declare that they have no known competing financial interests or personal relationships that could have appeared to influence the work reported in this paper.

Acknowledgements

W. Zhang, K. Zha, Y. Xiong, W. Hu contributed equally to this work. This work was supported by the National Science Foundation of China (No. 82272491, No. 82072444); the Wuhan Science and Technology Bureau (2022020801020464); the Department of Science and Technology of Hubei Province (No. 2021CFB425); Chinese Pharmaceutical Association Hospital Phamacy department (No. CPA-Z05-ZC-2022-002); Grants from Hubei Province Unveiling Science and Technology Projects (No. 2022-35).

Appendix A. Supplementary data

Supplementary data to this article can be found online at https://doi.org/10.1016/j.bioactmat.2023.07.006.

References

[1] J.B. Cole, J.C. Florez, Nat. Rev. Nephrol. 16 (7) (2020) 377–390, https://doi.org/10.1038/s41581-020-0278-5.
[2] S. Maschalidi, P. Mehrotra, B.N. Keceli, H.K.L. De Cleene, K. Lecomte, R. Van der Cruyssen, P. Janssen, J. Pinney, G. van Loo, D. Elewaut, A. Massie, E. Hoste, K. S. Ravichandran, Nature 606 (7915) (2022) 776–784, https://doi.org/10.1038/s41586-022-04754-6.
[3] Y. Xiong, L. Chen, P. Liu, T. Yu, C. Lin, C. Yan, Y. Hu, W. Zhou, Y. Sun, A.C. Panayi, F. Cao, H. Xue, L. Hu, Z. Lin, X. Xie, X. Xiao, Q. Feng, B. Mi, G. Liu, Small 18 (1) (2022), e2104229, https://doi.org/10.1002/smll.202104229.
[4] Y. Liang, J. He, B. Guo, ACS Nano 15 (8) (2021) 12687–12722, https://doi.org/10.1021/acsnano.1c04206.
[5] W. Mu, Q. Chu, Y. Liu, N. Zhang, Nano-Micro Lett. 12 (1) (2020) 142, https://doi.org/10.1007/s40820-020-00482-6.
[6] W. Shi, B. Hass, M.A. Kuss, H. Zhang, S. Ryu, D. Zhang, T. Li, Y.L. Li, B. Duan, Carbohydr. Polym. 233 (2020), 115803, https://doi.org/10.1016/j.carbpol.2019.115803.
[7] Y. Liang, M. Li, Y. Yang, L. Qiao, H. Xu, B. Guo, ACS Nano 16 (2) (2022) 3194–3207, https://doi.org/10.1021/acsnano.1c11040.
[8] Y. Xiong, B.B. Mi, Z. Lin, Y.Q. Hu, L. Yu, K.K. Zha, A.C. Panayi, T. Yu, L. Chen, Z. P. Liu, A. Patel, Q. Feng, S.H. Zhou, G.H. Liu, Mil Med Res 9 (1) (2022) 65, https://doi.org/10.1186/s40779-022-00426-8.
[9] C. Huang, L. Dong, B. Zhao, Y. Lu, S. Huang, Z. Yuan, G. Luo, Y. Xu, W. Qian, Clin. Transl. Med. 12 (11) (2022), e1094, https://doi.org/10.1002/ctm2.1094.
[10] E.A. Grice, E.S. Snitkin, L.J. Yockey, D.M. Bermudez, N.C.S. Program, K.W. Liechty, J.A. Segre, Proc. Natl. Acad. Sci. U. S. A. 107 (33) (2010) 14799–14804, https://doi.org/10.1073/pnas.1004204107.
[11] Q. Ding, T. Sun, W. Su, X. Jing, B. Ye, Y. Su, L. Zeng, Y. Qu, X. Yang, Y. Wu, Z. Luo, X. Guo, Adv Healthc Mater 11 (12) (2022), e2102791, https://doi.org/10.1002/adhm.202102791.
[12] Y. Liang, Y. Liang, H. Zhang, B. Guo, Asian J. Pharm. Sci. 17 (3) (2022) 353–384, https://doi.org/10.1016/j.ajps.2022.01.001.
[13] J. Winkler, S. Ghosh, J. Diabetes Res. 2018 (2018), 5391014, https://doi.org/10.1155/2018/5391014.
[14] Y. Zhao, P. Paderu, G. Delmas, E. Dolgov, M.H. Lee, M. Senter, S. Park, S. Leivers, D.S. Perlin, J. Trauma Acute Care Surg. 79 (4 Suppl 2) (2015) S121–S129, https://doi.org/10.1097/TA.0000000000000737.
[15] L. Sherry, E. Millhouse, D.F. Lappin, C. Murray, S. Culshaw, C.J. Nile, G. Ramage, BMC Oral Health 13 (2013) 47, https://doi.org/10.1186/1472-6831-13-47.
[16] G. Wang, F. Yang, W. Zhou, N. Xiao, M. Luo, Z. Tang, Biomed. Pharmacother. 157 (2023), 114004, https://doi.org/10.1016/j.biopha.2022.114004.
[17] H.J. Forman, H. Zhang, Nat. Rev. Drug Discov. 20 (9) (2021) 689–709, https://doi.org/10.1038/s41573-021-00233-1.
[18] M. Schafer, S. Werner, Pharmacol. Res. 58 (2) (2008) 165–171, https://doi.org/10.1016/j.phrs.2008.06.004.
[19] H.J. Forman, M. Maiorino, F. Ursini, Biochemistry 49 (5) (2010) 835–842, https://doi.org/10.1021/bi9020378.
[20] A.G. Manford, E.L. Mena, K.Y. Shih, C.L. Gee, R. McMinimy, B. Martinez-Gonzalez, R. Sherriff, B. Lew, M. Zoltek, F. Rodriguez-Perez, M. Woldesenbet, J. Kuriyan, M. Rape, Cell 184 (21) (2021) 5375–5390, https://doi.org/10.1016/j.cell.2021.09.002, e16.
[21] A.G. Manford, F. Rodriguez-Perez, K.Y. Shih, Z. Shi, C.A. Berdan, M. Choe, D. V. Titov, D.K. Nomura, M. Rape, Cell 183 (1) (2020) 46–61 e21, https://doi.org/10.1016/j.cell.2020.08.034.
[22] N.J. Henning, A.G. Manford, J.N. Spradlin, S.M. Brittain, E. Zhang, J.M. McKenna, J.A. Tallarico, M. Schirle, M. Rape, D.K. Nomura, J. Am. Chem. Soc. 144 (2) (2022) 701–708, https://doi.org/10.1021/jacs.1c03980.
[23] M. Sadeghi, B. Heidari, Materials 4 (3) (2011) 543–552, https://doi.org/10.3390/ma4030543.
[24] A.V.A. Mariadoss, A.S. Sivakumar, C.H. Lee, S.J. Kim, Biomed. Pharmacother. 151 (2022), 113134, https://doi.org/10.1016/j.biopha.2022.113134.
[25] P. Chakma, D. Konkolewicz, Angew Chem. Int. Ed. Engl. 58 (29) (2019) 9682–9695, https://doi.org/10.1002/anie.201813525.
[26] B. Marco-Dufort, J. Willi, F. Vielba-Gomez, F. Gatti, M.W. Tibbitt, Biomacromolecules 22 (1) (2021) 146–157, https://doi.org/10.1021/acs.biomac.0c00895.
[27] H. Sies, Redox Biol. 4 (2015) 180–183, https://doi.org/10.1016/j.redox.2015.01.002.
[28] N. Mariappan, C.M. Elks, S. Sriramula, A. Guggilam, Z. Liu, O. Borkhsenious, J. Francis, Cardiovasc. Res. 85 (3) (2010) 473–483, https://doi.org/10.1093/cvr/cvp305.
[29] T. Hussain, B. Tan, G. Murtaza, G. Liu, N. Rahu, M. Saleem Kalhoro, D. Hussain Kalhoro, T.O. Adebowale, M. Usman Mazhar, Z.U. Rehman, Y. Martinez, S. Akber Khan, Y. Yin, Pharmacol. Res. 152 (2020), 104629, https://doi.org/10.1016/j.phrs.2020.104629.
[30] H. Brem, M. Tomic-Canic, J. Clin. Invest. 117 (5) (2007) 1219–1222, https://doi.org/10.1172/JCI32169.
[31] V. Falanga, Lancet 366 (9498) (2005) 1736–1743, https://doi.org/10.1016/S0140-6736(05)67700-8.
[32] A.P. Veith, K. Henderson, A. Spencer, A.D. Sligar, A.B. Baker, Adv. Drug Deliv. Rev. 146 (2019) 97–125, https://doi.org/10.1016/j.addr.2018.09.010.